Published in final edited form as:
Ann Thorac Surg. 2011 January ; 91(1): 157–164. doi:10.1016/j.athoracsur.2010.09.078.

Ischemic Mitral Regurgitation: A Quantitative Three-Dimensional Echocardiographic Analysis

Mathieu Vergnat, MD, **Arminder S. Jassar, MBBS**, **Benjamin M. Jackson, MD**, **Liam P. Ryan, MD**, **Thomas J. Eperjesi, BS**, **Alison M. Pouch, BS**, **Stuart J. Weiss, MD, PhD**, **Albert T. Cheung, MD**, **Michael A. Acker, MD**, **Joseph H. Gorman III, MD**, and **Robert C. Gorman, MD**
Departments of Surgery and Anesthesia, and the Gorman Cardiovascular Research Group, University of Pennsylvania, Philadelphia, Pennsylvania

Abstract

Background—A comprehensive three-dimensional echocardiography based approach is applied to preoperative mitral valve (MV) analysis in patients with ischemic mitral regurgitation (IMR). This method is used to characterize the heterogeneous nature of the pathologic anatomy associated with IMR.

Methods—Intraoperative real-time three-dimensional transesophageal echocardiograms of 18 patients with IMR (10 with anterior, 8 with inferior infarcts) and 17 patients with normal MV were analyzed. A customized image analysis protocol was used to assess global and regional determinants of annular size and shape, leaflet tethering and curvature, relative papillary muscle anatomy, and anatomic regurgitant orifice area.

Results—Both mitral annular area and MV tenting volume were increased in the IMR group as compared with patients with normal MV (mitral annular area = 1,065 ± 59 mm^2 versus 779 ± 44 mm^2, $p = 0.001$; and MV tenting volume = 3,413 ± 403 mm^3 versus 1,696 ± 200 mm^3, $p = 0.001$, respectively). Within the IMR group, patients with anterior infarct had larger annuli (1,168 ± 99 mm^2) and greater tenting volumes (4,260 ± 779 mm^3 versus 2,735 ± 245 mm^3, $p = 0.06$) than the inferior infarct subgroup. Papillary-annular distance was increased in the IMR group relative to normal; these distances were largest in patients with anterior infarcts. Whereas patients with normal MV had very consistent anatomic determinants, annular shape and leaflet tenting distribution in the IMR group were exceedingly variable. Mean anatomic regurgitant orifice area was 25.8 ± 3.0 mm^2, and the number of discrete regurgitant orifices varied from 1 to 4.

Conclusions—Application of custom analysis techniques to three-dimensional echocardiography images allows a quantitative and systematic analysis of the MV, and demonstrates the extreme variability in pathologic anatomy that occurs in patients with severe IMR.

Ischemic mitral regurgitation (IMR) occurs when a structurally normal mitral valve (MV) is rendered incompetent as a result of myocardial infarction induced left ventricular (LV) remodeling [1]. Ischemic mitral regurgitation is present to some degree in 1.6 to 2.8 million Americans and in more than 50% of patients with reduced LV ejection fraction (<40%) who undergo coronary artery bypass grafting [2,3]. Ischemic mitral regurgitation increases mortality even when mild, with a strong graded relationship between severity and reduced survival [4]. Mitral valve repair with ring annuloplasty, typically performed in conjunction

Address correspondence to Dr R. C. Gorman, Gorman Cardiovascular Research Group, Glenolden Research Laboratory, University of Pennsylvania, 500 S Ridgeway Ave, Glenolden, PA 19036; gormanr@uphs.upenn.edu..

with coronary revascularization, has become the preferred treatment for IMR. However, this therapeutic approach is associated with recurrence of significant IMR in as many as 30% of patients at 6 months and as many as 60% of patients 3 to 5 years after surgery [5–7]. This lack of durability likely contributes to the difficulty in demonstrating a survival advantage for MV repair compared with medical management or revascularization alone in patients with IMR [6,7].

Laboratory [8,9] and clinical studies [10] have demonstrated that IMR is associated with changes in annular size, annular shape, and leaflet tethering. The inconsistent clinical response to annuloplasty strongly suggests that there is significant variability in how each of these variables contributes to MV incompetence in individual patients. We postulate that a more effective means to characterize the pathologic anatomy of the mitral valve complex in individual subjects would represent an initial step toward a patient-specific therapeutic approach to IMR and improved surgical outcomes.

In this report, we utilize a real-time three-dimensional echocardiography (rt-3DE) approach [11] to preoperative mitral valve analysis in patients with IMR. The method is used to quantitatively characterize the heterogeneous nature of the pathologic anatomy that is associated with the IMR clinical phenotype.

Patients and Methods

Patients

The intraoperative rt-3D transesophageal echocardiograms of 35 patients were analyzed. Eighteen patients with ischemic mitral regurgitation who were referred for mitral valve repair and surgical revascularization (IMR group) and 17 patients referred for nonmitral valve cardiac surgery with normal mitral valve function (normal group) were included in the study (Table 1). The protocol was approved by the University of Pennsylvania School of Medicine Institutional Review Board. All IMR patients had confirmed coronary artery disease, a discrete LV wall motion abnormality on visual assessment using the 16-segment model and scoring system established by the American Society of Echocardiography [12], and absence of leaflet pathology. Patients in the normal group had normal-appearing MV leaflets and no evidence of MR or wall motion abnormalities.

All patients had rt-3D transesophageal echocardiography in the operating room after general anesthesia had been induced but before the chest was opened. Electrocardiographically gated, full-volume data sets were acquired through midesophageal view, with an iE-33 platform (Philips Medical Systems, Andover, MA) equipped with a 2 to 7 MHz X7-2t transesophageal echocardiography matrix-array transducer. Care was taken to include the mitral apparatus in its entirety throughout the acquisition. The volumetric frame rate was set to 17 Hz to 30 Hz with an imaging depth of 12 cm to 16 cm.

Image Segmentation

All analysis was performed at midsystole. The mitral valve was segmented and analyzed as previously described [11]. Briefly, each full-volume data set was exported to an Echo-View 5.4 (TomTec Imaging Systems, Munich, Germany) software workstation for analysis. Images were rotated to allow orthogonal visualization of the left ventricle long-axis. Based on a uniform rotational template, 36 discrete points were interactively defined to delineate the annulus (Fig 1A). Freehand curves were constructed along the leaflet surface to independently identify the anterior and the posterior leaflets and the coaptation zone. This process was repeated at 1-mm intervals along the intercommissural axis to encompass the entire valve (Fig 1B). Anterior and posterior commissures were defined as annular points at the junction between the anterior and posterior leaflets (middle of commissural region).

Anterior and posterior papillary muscles tips were also indentified. Using a rotational template centered at the anterior horn, the regurgitant orifice was delineated along the coaptation region at 5-degree increments (Fig 1C).

Annular Analysis

Using custom Matlab algorithms (Mathworks, Natick, MA) and orthogonal distance regression, the least squares plane of the data point cloud for the annulus was aligned to the x-y plane. Under these geometric conditions, the annular height for each point (z_n) was plotted as a function of rotational position on the annulus. A number of anatomic landmarks (Fig 2) were identified. The septum was identified as the anterior horn of the annulus at the aortic valve, corresponding to z_{max}. The lateral annulus was located at the middle of the posterior annulus circumference. With the annular model transformed such that the commissures were aligned with the y-axis, the anterolateral and posteromedial annular points are the locations of maximal and minimal y-value.

Annular height was defined as z_{max} minus z_{min}. Septolateral diameter was defined as the distance, in three-dimensional space, separating the two data points, septum and lateral annulus. Commissural width was defined as the three-dimensional distance between the two commissures. Mitral transverse diameter was defined as the three-dimensional distance separating the anterolateral annulus and the posteromedial annulus. Mitral annular area was defined as the area enclosed by the two-dimensional projection of a given annular data set onto its least squares plane. Total mitral annular circumference and the lengths of the anterior and posterior annuli were calculated.

Leaflet and Papillary Muscle Analysis

The mitral valve tenting area (MVTa) was defined as the area enclosed by the mitral leaflets and the plane of the mitral annulus for a given point along the intercommissural axis (Fig 3). The MVTa was calculated at known intervals, Δc, along the intercommissural axis. The mitral valve tenting volume (MVTv) was calculated as the sum of the incremental regional volumes ($MVTa_n \times \Delta c_n$). The mitral valve tenting index (MVTI [MVTv divided by mitral annular area]) was also calculated for each data set [13]. To allow for intersubject comparison, intercommissural position was expressed as a percentage of the distance traveled between the anterior commissure and the posterior commissure, where 0% indicated the position of the anterior commissure and 100% indicated the position of the posterior commissure [14]. The papillary-annuls distance was determined as the distance between each papillary muscle tip and the center of the mitral annulus. The distance between each papillary muscle tip and its ipsilateral and contralateral commissure was also calculated. Three-dimensional leaflet Gaussian curvature (K) was assessed using previously published methodology [15]. Color contour plots, determined by the value of K, were then rendered for each subject, depicting curvature at every point on the leaflet.

Statistical Analyses

All values are expressed as mean ± SE. Student's *t* tests were computed for all comparisons, and *p* values of 0.05 or less were considered significant. All statistical analysis was performed using SPSS software (SPSS, Chicago, IL).

Results

Measured and derived annular and leaflet determinants are summarized in Table 2.

Annular Size

The IMR group had significantly larger mitral annular area (779 ± 44 mm^2 versus 1,065 ± 59 mm^2, $p = 0.001$) and annular circumference (121.6 ± 3.1 mm versus 102.3 ± 3.0 mm, $p = 0.0001$) when compared with the normal group. Most of the increase in annular circumference was due to expansion of the length of posterior annulus (79.9 ± 1.9 mm in the IMR group versus 64.1 ± 2.3 mm in normal subjects, $p = 10^{-6}$). Both the maximum transverse diameter (34.4 ± 1.1 mm versus 38.8 ± 1.0 mm, $p = 0.007$) and the septolateral dimension (28.6 ± 0.9 mm versus 34.0 ± 1.2 mm, $p = 0.002$) were increased in the IMR group. When IMR patients with anterior and inferior infarcts were compared, all indices of annular size were larger in the anterior infarct subgroup. The length of the posterior annulus was greater in the anterior infarct subgroup (84.2 ± 2.2 mm versus 76.4 ± 2.5 mm, $p = 0.04$), and there was a trend toward larger annular size in patients with anterior infarcts (1,168 ± 99 mm^2 versus 982 ± 63 mm^2, $p = 0.1$).

Annular Shape

All patients in the normal group had saddle-shaped annuli. Annular shape in the IMR group, however, varied widely (Fig 4). Some IMR patients had normal appearing saddle-shaped annuli (Fig 4B) whereas others had virtually flat annuli (Fig 4C). Annular restriction toward the LV cavity was common along the posterior annulus in both infarct subgroups (Fig 4A), with some patients manifesting a single area of annular restriction (Fig 4D) whereas other patients had two or more regions where the posterior annulus was restricted into the LV (Fig 4E). While inferior annular restriction was present in both anterior and inferior infarct groups, the depth of both commissures was decreased for anterior infract cohort, resulting in a flatter annulus.

Leaflet Tethering

The mitral valve tenting volume was increased in the IMR group compared with the control group (3,413 ± 403 mm^3 versus 1,696 ± 200 mm^3, $p = 0.001$). Within IMR group, the increase in tenting volume was more pronounced in the anterior infarct subgroup (4,260 ± 779 mm^3 versus 2,735 ± 245 mm^3 for the inferior subgroup, $p = 0.06$). The degree and distribution of leaflet tethering varied extensively in the IMR group (Fig 3, Fig 5B to E). The area of peak tenting along the intercommissural annular axis also varied extensively (Fig 5A) and tended to be shifted toward the posterior commissure in the anterior infarct subgroup.

Subvalvular Anatomic Relationships

Table 2 depicts differences in annular-papillary muscle relationships between normal and IMR groups. All distances were increased in the IMR group compared with the normal group. The largest differences between IMR and normal groups occurred in the interpapillary muscle distance (33.7 ± 1.6 mm versus 24.7 ± 1.2 mm, $p = 0.0001$), posterior papillary muscle to anterior commissure distance (46.0 ± 2 mm versus 37.7 ± 1.5 mm, $p = 0.003$), and the posterior papillary muscle to posterior commissure distance (35.2 ± 1.6 mm versus 28.7 ± 1.0 mm). Again, all indices of subvalvular remodeling were largest in the anterior infarct subgroup.

Leaflet Curvature

Representative patterns of three-dimensional leaflet curvature are shown in Figure 6. Prominent elliptic regions (curvature “hotspots”) within the anterior leaflet consistent with leaflet convexity toward the LV cavity were found in 17 of the 18 IMR patients. In 11 of these patients, there were two curvature hotspots symmetrically distributed around a hyperbolic region in the center of the anterior leaflet (Fig 6A). In 6 patients, there was one

prominent curvature hot spot located centrally in the anterior leaflet (Fig 6B). These high Gaussian curvature foci varied in intensity from 1.14 mm^{-1} to 4.07 mm^{-1}. None of patients in the normal group had significant leaflet curvature hotspots (Fig 6C, D). The location and orientation of the areas of intense positive Gaussian curvature suggest that they may result from secondary chordal tethering of the anterior leaflet.

Regurgitant Orifice

It was possible to delineate the regurgitant orifice in 16 of 18 IMR patients. Although the degree of mitral regurgitation was similar in all patients, the distribution and size of the regurgitant area varied substantially. Mean regurgitant orifice area was 25.8 ± 3.0 mm^2 (8.5 mm^2 to 46.8 mm^2). Five IMR patients had one regurgitant orifice; 10 patients had 2 distinct regurgitant orifices and 1 patient had 4 distinct regurgitant zones (Fig 7).

Comment

Real-time 3DE technology is becoming commonplace in operating rooms and provides spectacular visual images of the mitral valve. However, the application of 3DE to quantify MV annular and subvalvular changes that occur with IMR has been limited. The aim of this study was to use a custom rt-3DE based analysis technique to better elucidate of the pathologic anatomy that leads to valve incompetence in IMR patients. Our findings demonstrate that extreme variability is present in pathologic anatomy within a seemingly homogenous clinical cohort of patients with severe IMR. It has been widely accepted that IMR is associated with annular and subvalvular remodeling that is manifest by annular dilation [16,17], annular shape change [9,18], and leaflet tethering [19,20]. While all IMR patients in this study manifested some degree of annular dilation, annular size and shape varied widely. Although some patients maintain a nearly normal saddle-shaped annulus, others suffer from severe annular flattening. Also interesting is the extensive regional variation in annular shape that was demonstrated in the region of the posterior annulus (Fig 4).

Extreme anatomic variability was also found in the extent and distribution of mitral leaflet tethering. Tenting volumes varied from near normal to severely tethered geometry (Figs 3 and 5). The tenting distribution pattern across the valve was also found to vary from normal symmetrical tenting distribution to cases where tenting was skewed toward either the anterior or posterior commissure (Fig 5). These observations suggest that obtaining measurements such as tenting area, tenting height, leaflet tenting angles, and coaptation length using two-dimensional echocardiography may produce inconsistent results even within an individual patient based on the location of the selected imaging plane.

Patients with anterior infarcts had larger annuli and more extensive perturbations in papillary-annular dimensions, suggesting that anterior infarcts result in IMR only after extensive LV remodeling has already occurred whereas IMR occurs earlier in the posterior infarct remodeling process.

Variability was also present in the degree of leaflet curvature (Fig 6). Gaussian curvature maps revealed a heterogeneous pattern of curvature hotspots within the anterior leaflet. If future work substantiates our hypothesis that these hotspots indeed represent areas of secondary chordal tethering, this analysis would aid surgeons who utilize secondary chordal transection as part of their repair strategy for IMR patients.

For the first time, we demonstrate a technique to directly assess the location and size of the anatomic regurgitant orifice area in patients with IMR. With increased clinical experience, this type of data may represent a load-independent method for quantifying the degree of

IMR as well as a patient's response to annuloplasty. Again, the results of this analysis emphasize the heterogeneous nature of IMR with regurgitant area that varied from 8.5 mm^2 to 46.8 mm^2 and the number of discrete regurgitant orifices varying from 1 to 4 (Fig 7).

As described above, the pathologic three-dimensional anatomy of IMR is complex and varies extensively between patients. The most widely accepted surgical approach to IMR is undersized ring annuloplasty. Annuloplasty, while effective in reducing annular area, does little to improve and may actually exacerbate leaflet tethering [21], potentially contributing to the high incidence of recurrent IMR after surgical repair. The ability to quantitatively determine the relative contribution of annular dilation and leaflet tethering to IMR in the individual patient would help surgeons decide between valve replacement, simple repair with annuloplasty alone or in combination with more complex repair techniques like chordal transection, leaflet augmentation, or papillary muscle repositioning. It has been demonstrated that coaptation and tenting determinants vary significantly within different regions of the mitral valve in patients with IMR [22]. It thus stands to reason that isolated single-plane indices of leaflet tethering and annular remodeling obtained with two-dimensional echocardiography are insufficient to allow a patient-specific approach to IMR and to accurately predict durability of repair, which may explain current high rates of recurrent IMR.

Experienced mitral valve surgeons have emphasized the importance of direct “valve analysis” in the operating room as an important diagnostic component of the mitral valve repair process. We believe that with increased clinical experience, the approach reported here will provide the surgeon with the ability to perform a detailed, in vivo dynamic three-dimensional valve analysis preoperatively and help direct surgical intent to either mitral valve repair or replacement.

Acknowledgments

This research project was supported by grants from the National Heart, Lung, and Blood Institute of the National Institutes of Health, Bethesda, Maryland (HL63954 and HL73021). Drs Robert Gorman and Joseph Gorman are supported by individual Established Investigator Awards from the American Heart Association, Dallas, Texas. Dr. Jassar is supported by a postdoctoral fellowship from the American Heart Association. Dr. Vergnat was supported by a French Federation of Cardiology Research Grant.

References

1. Gorman, RC.; Gorman, JH.; Edmunds, LH. Ischemic mitral regurgitation.. In: Cohn, LH.; Edmunds, LH., editors. Cardiac surgery in the adult. 2nd edn.. McGraw-Hill; New York: 2003. p. 751-69.
2. Borger MA, Alam A, Murphy PM, Doenst T, David TE. Chronic ischemic mitral regurgitation: repair, replace or rethink? Ann Thorac Surg 2006;81:1153–61. [PubMed: 16488757]
3. Trichon BH, Felker GM, Shaw LK, Cabell CH, O'Connor CM. Relation of frequency and severity of mitral regurgitation to survival among patients with left ventricular systolic dysfunction and heart failure. Am J Cardiol 2003;91:538–43. [PubMed: 12615256]
4. Grigioni F, Enriquez-Sarano M, Zehr KJ, Bailey KR, Tajik AJ. Ischemic mitral regurgitation: long-term outcome and prognostic implications with quantitative doppler assessment. Circulation 2001;103:1759–64. [PubMed: 11282907]
5. McGee EC, Gillinov AM, Blackstone EH, et al. Recurrent mitral regurgitation after annuloplasty for functional ischemic mitral regurgitation. J Thorac Cardiovasc Surg 2004;128:916–24. [PubMed: 15573077]
6. Crabtree TD, Bailey MS, Moon MR, et al. Recurrent mitral regurgitation and risk factors for early and late mortality after mitral valve repair for functional ischemic mitral regurgitation. Ann Thorac Surg 2008;85:1537–43. [PubMed: 18442534]

7. De Bonis M, Lapenna E, Verzini A, et al. Recurrence of mitral regurgitation parallels the absence of left ventricular reverse remodeling after mitral repair in advanced dilated cardiomyopathy. Ann Thorac Surg 2008;85:932–9. [PubMed: 18291174]
8. Gorman RC, McCaughan JS, Ratcliffe MB, et al. Pathogenesis of acute ischemic mitral regurgitation in three dimensions. J Thorac Cardiovasc Surg 1995;109:684–93. [PubMed: 7715215]
9. Gorman JH, Gorman RC, Jackson BM, Enomoto Y, St. John Sutton MG, Edmunds LH. annuloplasty ring selection for chronic ischemic mitral regurgitation: lessons from the ovine model. Ann Thorac Surg 2003;76:1556–63. [PubMed: 14602285]
10. Otsuji Y, Handschumacher MD, Liel-Cohen N, et al. Mechanism of ischemic mitral regurgitation with segmental left ventricular dysfunction: three-dimensional echocardiographic studies in models of acute and chronic progressive regurgitation. J Am Coll Cardiol 2001;37:641–8. [PubMed: 11216991]
11. Jassar AS, Brinster CJ, Vergnat M, et al. Quantitative mitral valve modeling using real-time three-dimensional echocardiography: technique and repeatability. Ann Thorac Surg 2011;91:165–71. [PubMed: 21172507]
12. Shanewise JS, Cheung AT, Aronson S, et al. ASE/SCA guidelines for performing a comprehensive intraoperative multiplane transesophageal echocardiography examination: recommendations of the American Society of Echocardiography Council for Intraoperative Echocardiography and the Society of Cardiovascular Anesthesiologists Task Force for Certification in Perioperative Transesophageal Echocardiography. Anesth Analg 1999;89:870–84. [PubMed: 10512257]
13. Ryan LP, Jackson BM, Parish LM, et al. Mitral valve tenting index for assessment of subvalvular remodeling. Ann Thorac Surg 2007;84:1243–9. [PubMed: 17888976]
14. Ryan LP, Jackson BM, Parish LM, et al. Quantification and localization of mitral valve tenting in ischemic mitral regurgitation using real-time three-dimensional echocardiography. Eur J Cardiothorac Surg 2007;31:839–44. [PubMed: 17329114]
15. Ryan LP, Jackson BM, Eperjesi TJ, et al. A methodology for assessing human mitral leaflet curvature using real-time 3-dimensional echocardiography. J Thorac Cardiovasc Surg 2008;136:726–34. [PubMed: 18805278]
16. Gorman JH, Jackson BM, Enomoto Y, Gorman RC. The effect of regional ischemia on mitral valve annular saddle shape. Ann Thorac Surg 2004;77:544–8. [PubMed: 14759435]
17. Levine RA, Schwammenthal E. Ischemic mitral regurgitation on the threshold of a solution: from paradoxes to unifying concepts. Circulation 2005;112:745–58. [PubMed: 16061756]
18. Watanabe N, Ogasawara Y, Yamaura Y, et al. Mitral annulus flattens in ischemic mitral regurgitation: geometric differences between inferior and anterior myocardial infarction. A real-time 3-dimensional echocardiographic study. Circulation 2005;112(Suppl 1):458–62.
19. Yiu SF, Enriquez-Sarano M, Tribouilloy C, et al. Determinants of the degree of functional mitral regurgitation in patients with systolic left ventricular dysfunction: a quantitative clinical study. Circulation 2000;102:1400–7. [PubMed: 10993859]
20. Calafiore AM, Gallina S, Di Mauro M, et al. Mitral valve procedure in dilated cardiomyopathy: repair or replacement? Ann Thorac Surg 2001;71:1146–53. [PubMed: 11308151]
21. Kuwahara E, Otsuji Y, Iguro Y, et al. Mechanism of recurrent/persistent ischemic/functional mitral regurgitation in the chronic phase after surgical annuloplasty: importance of augmented posterior leaflet tethering. Circulation 2006;114(Suppl 1):529–34.
22. Gogoladze G, Dellis SL, Donnino R, et al. Analysis of mitral coaptation zone in normal and functional regurgitant valves. Ann Thorac Surg 2010;89:1158–61. [PubMed: 20338324]

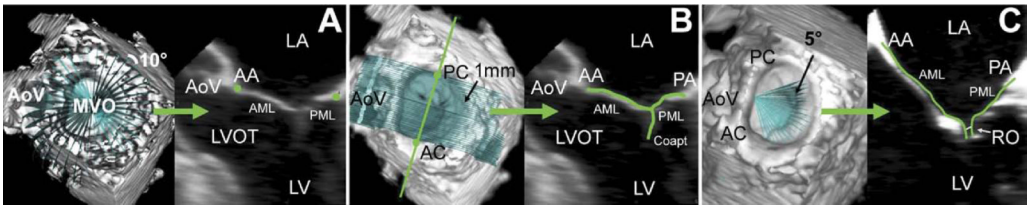

Fig 1.

Annular and leaflet segmentation. (A) Annular delineation using rotational cross-sections at 10-degree increments, centered on the geometric center of the mitral valve. (B) Leaflet segmentation using transverse cross-sections every 1 mm along intercommissural axis. (C) Regurgitant orifice delineation using rotational cross-sections at 5-degree increments, centered on the aortomitral junction. In each panel, the three-dimensionally rendered echocardiographic volume containing the mitral valve is displayed on the left, with cross-sectional planes; the two-dimensional resulting cross-section is displayed on the right. (AA = anterior annulus; AC = anterior commissure; AML = anterior mitral leaflet; AoV = aortic valve; Coapt = coaptation; LA = left atrium; LV = left ventricle; LVOT = left ventricular outflow tract; MVO = mitral valve orifice; PA = posterior annulus; PC = posterior commissure; PML = posterior mitral leaflet; RO = regurgitant orifice.)

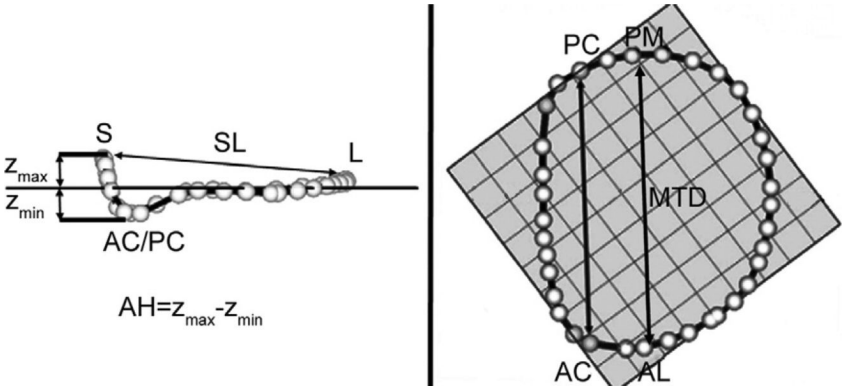

Fig 2.

Annular modeling. (A) Intercommissural and (B) transvalvular views of a real-time three-dimensional echocardiography derived mitral annular model are depicted. The least squares plane has been superimposed on the annulus in each view. (A) The manner in which the annular height (AH) and septolateral diameter (SL) are determined is illustrated. (B) The manner in which the intercommissural width (CW) and the mitral transverse diameter (MTD) are determined is illustrated. (AC = anterior commissure; AL = anterolateral annulus; L = lateral annulus; PC = posterior commissure; PM = posteromedial; S = septum; Z_{max} = maximum annular height corresponding to septum; Z_{min} = minimum annular height.)

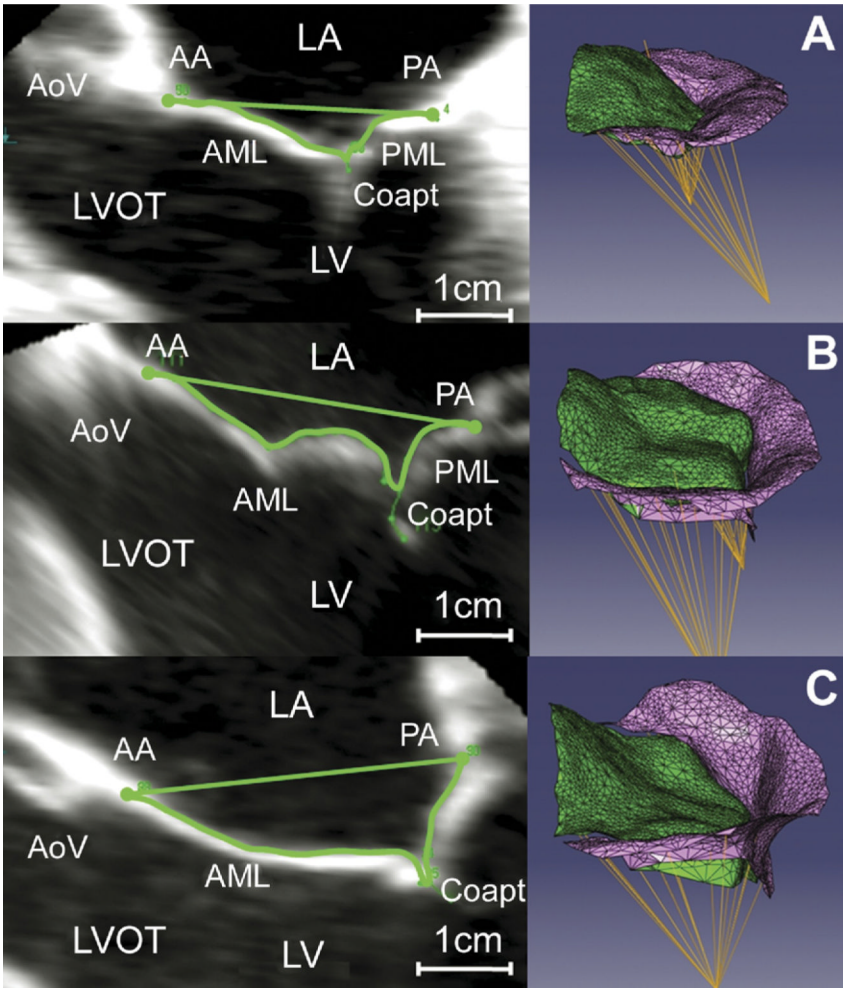

Fig 3.

Three-dimensional valve renderings. Mitral leaflet tethering for representative valves: (left) two-dimensional echocardiographic image with tenting area delineated; (right) three-dimensional rendering in an oblique view. (A) Normal valve, (B) ischemic mitral regurgitation (IMR) valve with limited tethering, and (C) IMR valve with severe leaflet tethering. (AA = anterior annulus; AML = anterior mitral leaflet; AoV = aortic valve; Coapt = coaptation; LA = left atrium; LV = left ventricle; LVOT = left ventricular outflow tract; PA = posterior annulus; PML = posterior mitral leaflet.)

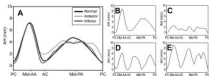

Fig 4.

Regional annular shape, presented as regional annular height (AH) plotted as a function of rotational position, averaged for (A) cohorts and for (B–E) selected ischemic mitral regurgitation patients. All patients' commissures were aligned in such a way that the posterior commissure (PC) was located at 0% and the anterior commissure (AC) at 33.3% of the rotational position along the annulus. Note the increased variability of AH in the posterior annular (PA) region. Also note the extremely variable annular shape, varying from normal (B) to flat (C), mid-posterior restriction (D), and bimodal posterior restriction (E). (AA = anterior annulus; PC = posterior commissure; black line = normal; dark gray line = inferior; light gray line = anterior.)

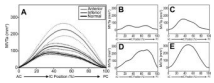

Fig 5.

Regional mitral valve tenting area (MVTa [tenting distribution]) plotted as a function of intercommissural (IC) position, expressed as a percentage of the distance traveled from the anterior commissure (AC). The positions of the AC and posterior commissure (PC) are, respectively, 0% and 100%. (A) Mean data (with SEM) for the normal cohort and ischemic mitral regurgitation (IMR) cohorts with either inferior or anterior infarcts. Note the shifting of the maximum tenting area toward PC with anterior infarct location. (B–E) Data for selected individual IMR patients are displayed. Note the variability in the extent and location of leaflet tenting. (Black line = normal; dark gray line = inferior; light gray line = anterior.)

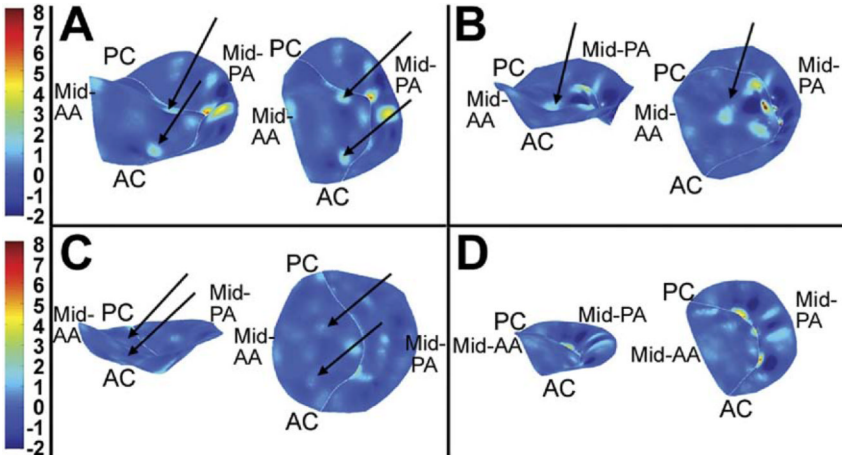

Fig 6.

Three-dimensional renderings of leaflet curvature. Color contouring is determined by three-dimensional leaflet Gaussian curvature (K). Negative K values indicate saddle-shaped (hyperbolic) local surface curvature; positive K values indicate elliptic local surface curvature but may be concave toward the left ventricle or left atrium. Valves are rendered as if the viewer were looking down from the left atrium. The left-hand image in each panel is oriented to allow appreciation of the three-dimensional directionality of positive Gaussian curvature (see text); the right-hand image is a two-dimensional planar projection of the leaflets. (A) A valve with two areas of intensive positive curvature convex toward the left ventricle; this was the most common configuration in the ischemic mitral regurgitation group. (B) A unifocal area of intense positive curvature is demonstrated. (C) A lesser degree of positive curvature foci is illustrated. (D) A healthy person with normal leaflet redundancy is shown. (AA = anterior annulus; AC = anterior commissure; PA = posterior annulus; PC = posterior commissure.)

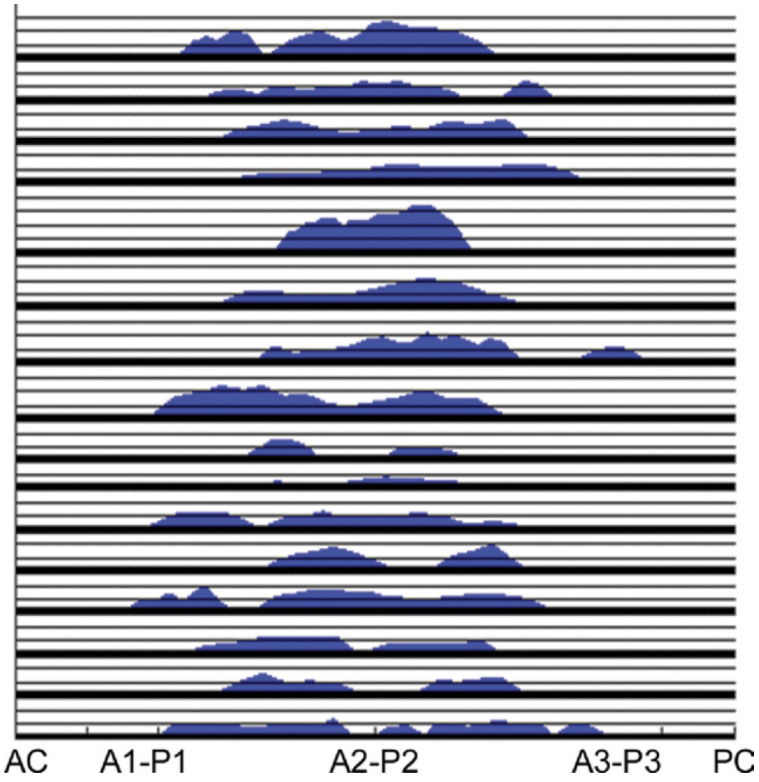

Fig 7.

Regurgitant orifice geometry, presented as orifice width plotted as a function of location along coaptation line (expressed as a percentage of the distance traveled from the anterior commissure). The positions of the anterior commissure (AC) and posterior commissure (PC) and valve segments (A1-P1 to A3-P3) are labeled. To avoid curves overlapping, all patients have been overlaid. Each vertical graduation represents 1-mm regurgitant width. Note extension of regurgitant orifice along the entire coaptation region and also the variable size and number of orifices.

Table 1

Patient Demographics

Parameter	IMR (n = 18)	Normal (n = 17)
Age, years	67 ± 11	65 ± 15
Ejection fraction, %	31 ± 13	63 ± 10
MR grade, 0–4 scale	3.1 ± 0.8	None
Jet direction		None
Inferior, %	67	
Central, %	23	
WMA location		None
Anterior, %	56	
Inferior, %	44	

Values are mean ± SD.

IMR = ischemic mitral regurgitation; MR = mitral regurgitation; WMA = wall motion abnormality.

Table 2

Mitral Valve and Subvalvular Anatomic Determinants

Determinant	Normal (n = 17)	IMR (n = 18)	Anterior MI (n = 8)	Inferior MI (n = 10)
Annular height, mm	7.5 ± 0.4	7.4 ± 0.4	6.8 ± 0.8	7.9 ± 0.4
Commissural width, mm	30.9 ± 0.9	33.5 ± 1.3	34.3 ± 2.6	32.8 ± 1.1
Septolateral diameter, mm	28.6 ± 0.9	34 ± 1.2[a]	36.1 ± 1.9[a]	32.3 ± 1.5[a]
Mitral transverse diameter, mm	34.4 ± 1.1	38.8 ± 1.0[a]	40.2 ± 1.9[a]	37.7 ± 1.0
Mitral annular area, mm^2	779 ± 44	1065 ± 59[a]	1168 ± 99[a]	982 ± 63[a]
MVT_V (mm^3	1696 ± 200	3413 ± 403[a]	4260 ± 779[a]	2735 ± 245[a]
Tenting index, mm	2.16 ± 0.20	3.13 ± 0.28[a]	3.48 ± 0.52[a]	2.85 ± 0.28[a]
Annular circumference, mm	102.3 ± 3.0	121.6 ± 3.1[a]	126.5 ± 5.4[a]	117.7 ± 3.3[a]
Length of anterior annulus, mm	38.2 ± 1.2	41.7 ± 2.0	42.3 ± 4.2	41.3 ± 1.4
Length of posterior annulus, mm	64.1 ± 2.3	79.9 ± 1.9[a]	84.2 ± 2.2[a]	76.4 ± 2.5[ab]
Interpapillary distance	24.7 ± 1.2	33.7 ± 1.6[a]	35.7 ± 2.5[a]	32.0 ± 2.0[a]
APM center	27.9 ± 0.9	30.6 ± 1.3	32.9 ± 2.4	28.7 ± 1.1
PPM center	27.8 ± 1.2	32.5 ± 1.4[a]	34.3 ± 2.6[a]	31.0 ± 1.4
APM-AC	26.2 ± 1.1	29.6 ± 1.4	32.1 ± 2.3[a]	27.7 ± 1.7
PPM-PC	28.7 ± 1.0	35.2 ± 1.6[a]	37.0 ± 2.7[a]	33.8 ± 1.8[a]
APM-PC	39.0 ± 1.2	43.5 ± 1.9	47.8 ± 3.0[a]	40.1 ± 1.8[b]
PPM-AC	37.7 ± 1.5	46.0 ± 2.0[a]	49.9 ± 3.1[a]	42.9 ± 2.2[a]

Values are mean ± SEM.

AC = anterior commissure; APM = anterior papillary muscle tip; IMR = ischemic mitral regurgitation; MI = myocardial infarction; MVT_V = mitral valve tenting volume; PC = posterior commissure; PPM = posterior papillary muscle tip.

[a] Statistically significant difference from normal.

[b] Significant difference from anterior myocardial infarction.